ACS OMEGA

http://pubs.acs.org/journal/acsodf

Article

Pseudouridimycin—A Potent Nucleoside Inhibitor of the RNA Polymerase Beta Prime Subunit of *Streptococcus pyogenes*

Kunthavai Pavundurai Chandra, Damodharan Perumal, and Preethi Ragunathan*

Cite This: *ACS Omega* 2023, 8, 7989−8000

Read Online

ACCESS | Metrics & More | Article Recommendations | Supporting Information

ABSTRACT: *Streptococcus pyogenes* (group A streptococcus, GAS), a Gram-positive bacterium, is a major cause of mild to severe life-threatening infections. Antibacterial resistance to penicillin and macrolides poses a major threat in the treatment of GAS and necessitates alternate drugs and newer antibiotics. In this direction, nucleotide-analog inhibitors (NIAs) have emerged as important antiviral, antibacterial, and antifungal agents. Pseudouridimycin (PUM), a nucleoside analogue inhibitor discovered from the soil bacterium *Streptomyces* sp., has proven to be effective against multidrug-resistant *S. pyogenes*. However, the mechanism of its activity remains elusive. In this study, subunits of the RNA polymerase of GAS have been identified as targets for PUM inhibition and the binding regions have been mapped to the N-terminal domain of the β' subunit, using computational methods. The antibacterial activity of PUM against macrolide-resistant GAS was evaluated. PUM showed effective inhibition at 0.1−1 μg/mL concentration, which was higher when compared to earlier reports. The molecular interaction between PUM and the RNA polymerase β'-N terminal subunit was investigated using isothermal titration calorimetry (ITC), circular dichorism (CD), and intrinsic fluorescence spectroscopy. The thermodynamic characterization by ITC showed an affinity constant of 6.175×10^5 M^{-1} denoting a moderate affinity. Fluorescence studies revealed that the interaction of protein-PUM was spontaneous in nature and follows a static quenching of tyrosine signals from the protein. The near- and far-UV CD spectral analysis concluded that PUM induced local tertiary structural changes in the protein, predominantly contributed by aromatic amino acids rather than notable changes in the secondary structure. Hence PUM could be a promising lead drug target for macrolide-resistant strains of *S. pyogenes* and enable eradication of pathogen in the host system.

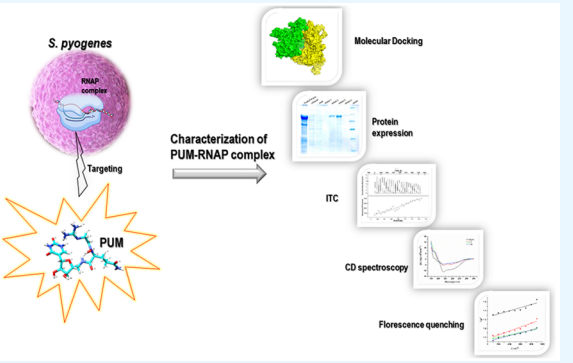

INTRODUCTION

A worldwide endemic outbreak by pathogens always poses a threat to humankind. Among pathogens, Gram-positive bacteria are of concern since they can cause life-threatening diseases. One of the well-known species of Gram-positive extracellular bacterial pathogens is *Streptococcus pyogenes* (group A streptococcus, GAS). Group A streptococci populate the skin or throat and possess sophisticated virulence mechanisms enabling escape from host defense mechanisms and causing bacterial pharyngitis, scarlet fever, and impetigo.[1] In a recent study, GAS pharyngitis was found to co-occur with COVID-19 infection, causing genuine concern about streptococcal diseases.[2] In light of this, internalization and intracellular survival offer a unique explanation for the ineffectiveness of penicillin. Further, incidence of macrolide resistance has been reported in GAS strains, pushing the edge to find new antibiotics or vaccine candidates to forestall disease mortality.[3]

Among various drug targets, bacterial RNA polymerases (bRNAPs) have been the most attractive for a multitude of broad-spectrum antibacterial therapies for three reasons: (a) the cruciality of the enzyme for bacterial survival, (b) highly conserved sequence similarity of the subunits across bacterial species, and (c) diversity of sequences among prokaryotes and eukaryotic RNA polymerases I, II, and III.[4] bRNAP inhibitors attach to the multienzyme complex at various sites, particularly the β' subunit, which harbors the active center. The well-known antibiotic Rifamycin and its derivatives, namely rifampicin, rifabutin, and rifamexyl (RMX), inhibit bacterial infection by sterically impeding the expansion of emerging RNA.[5] Streptolydigin, lipiarmycin, CBR hydroxamidines and their pyrazole derivatives inhibit the bRNAPs by averting the chain elongation and transcription initiation mechanism.[6,7] The notable cyclic peptide GE23077 targets active center i and i+1 sites, thus stalling the transcription process.[8] Apart from the active center, the switch regions of RNAPs have been targets for inhibitors such as myxopyronin, ripostatin,

Received: December 7, 2022
Accepted: February 1, 2023
Published: February 13, 2023

corallopyronin and squaramides.[9,10] Despite the fact that there are numerous bRNAP inhibitors, rifamycins and lipiarmycins are currently in clinical use to date.[11]

Apart from the conventional antibiotics, a new paradigm, nucleoside analogue inhibitors (NAIs), have demonstrated selective bacterial RNAP inhibition, imposing functional constraints by substituting RNAP nucleoside-triphosphate (NTP) binding sites and minimizing the substitutions that confer resistance.[12] These nucleoside analogues are routinely used to treat viral and fungal infections but have gained less attention as antibacterial compounds.[13] Most researchers believed that it would be impossible for a drug to specifically block the nucleoside triphosphate binding site of bacterial RNA polymerase because its sequence and structure are comparable to human RNA polymerase. In a recent discovery, pseudouridimycin (PUM), a new microbially synthesized nucleoside-analogue inhibitor of bacterial RNA polymerase with wide-ranging antibacterial action and a low rate of resistance acquisition has been reported.[14] Pseudouridimycin is selective because of its side chain that binds in a region that is conserved in bacterial RNA polymerases but not in humans. It is shown that PUM particularly inhibits bRNAP *in vitro*, with an IC_{50} of ∼0.1 μM and also with a minimum inhibitory concentration (MIC) of 4 to 6 μg/mL. *In vitro* bactericidal activity is reported for PUM against drug-sensitive, drug-resistant, and multidrug-resistant Streptococcus species. Further, PUM has been shown to clear *S. pyogenes* infection *in vivo* in a mouse peritonitis model. From the crystal structure of *Thermus thermophilus*, PUM was shown to strive for UTP occupancy and binds to the bRNAP NTP addition site.[15] Another interesting feature of PUM is that it did not exhibit any cross-resistance with the well-known clinical inhibitors. PUM binds to the NTP site, making it considerably more difficult for the bacteria to build resistance because blocking its binding would probably also abrogate RNAP activity. The *N*-hydroxy, glutamine, and guanidinyl moieties of PUM were shown to be crucial in preliminary lead-optimization studies (Figure 1). Any alteration or repression of these groups

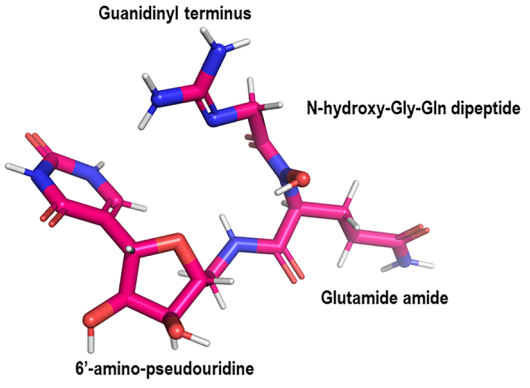

Figure 1. Structure of pseudouridimycin (PUM) showing the *N*-hydroxylated Gly-Gln dipeptide conjugated to 6′-amino-pseudouridine.

resulted in a sharp decline in activity while protection of the glutamine side-chain amide was tolerated.[16] Despite the enthusiasm of the discovery of a new antibiotic, molecular-level interactions of PUM with bRNAP have not been reported. Hence, an attempt has been made to show the actual binding nature of PUM. Here, we report the antibacterial activity of PUM against macrolide-resistant GAS and postulate a possible mechanism of PUM inhibition of RNAP in *S. pyogenes* through various biophysical and computational methods.

MATERIALS AND METHODS

Antibacterial Activity. The antibacterial activity of PUM against *S. pyogenes* was evaluated by the micro dilution method. Clinical samples obtained from the Voluntary Health Services (VHS), Adyar, Chennai, and standard cultures obtained from The Microbial Type Culture Collection and Gene Bank (MTCC) were grown in Mueller−Hinton broth (MHB) supplemented with 5% defibrinated sheep blood and used for the activity studies. The inoculum was prepared from a single colony in MHB liquid medium with 5% defibrinated sheep blood and incubated at 37 °C in a candle jar for 24−48 h. The derived bacterial suspension after 24 h was diluted to 10^8 CFU/mL (turbidity = McFarland barium sulfate standard 0.5) with sterile MHB medium. PUM was dissolved in sterile water to a final concentration of 1 mg/mL and further serially diluted in a 1:1 ratio to the concentrations ranging from 1 to 0.0156 μg/mL; 100 μL of each dilution was distributed in 96-well microtitration plates, along with sterility control (MHB alone) and growth control (MTCC culture). All the test and growth control wells were inoculated with 5 μL of bacterial suspension and the 96-well microtitration plates were incubated for 24 h in a candle jar at 37 °C. The experiments were performed in triplicate, and the microtitration plates were checked for inhibition by streaking each well in the MHB agar plate with 5% defibrinated sheep blood incubated at 37 °C for 24 h.

Molecular Docking. The mechanism of PUM binding to the RNAP complex has been studied by docking ligand with the RNAP beta (β) and beta prime (β′) subunits. The binding pocket of PUM was identified by comparing the RNA polymerase complex of *S. pyogenes* with the crystal structure of the *Thermus thermophilus* RNAP-PUM complex, retrieved from the PDB (PDB id: 5X21). A sequence alignment of the β and β′ prime subunits of *S. pyogenes* against those of *T. thermophilus* was carried out. The interacting residues were aligned and the binding pocket was identified in the modeled RNA polymerase β and β′ complex of *S. pyogenes*. The β and β′ subunits were docked using the HADDOCK web interface,[17] and the docked complex was subjected to hydrogen bond optimization and energy minimization using a protein preparation wizard under the OPLS-2005 (Optimized Potential for Liquid Simulations) force field.[18] The 3D coordinates of the ligand were generated using the Ligprep module,[19] and energy was minimized under the OPLS-2005 force field. The docking of ligand PUM with the β-β′ protein complex was carried out using the Induced Fit Docking (IFD) module of Schrödinger.[20] The best docked poses from 20 generated structures were chosen based on the glide energy, docking score, and favorable interactions.

Molecular Dynamics Simulation. The stability of the docked complex was assessed by performing a molecular dynamics (MD) simulation using GROMACS 2020.3.[21] The docked complex was placed in a solvated cubic box using the space point charge (SPC) water model at a distance of 1.0 nm for all atoms to the edge of the box. The topology file for the ligand was generated using the PRODRG server[22] followed by energy minimization of the complex for 500 steps by the steepest descent algorithm.[23] The β-β′-PUM complex was equilibrated using the Berendsen thermostat velocity with

https://doi.org/10.1021/acsomega.2c07805
ACS Omega 2023, 8, 7989−8000

NVT (constant number of particles, volume, and temperature).[24] For long-range electrostatics, the particle mesh Ewald (PME) coulomb followed by 1 ns NPT (constant number of particles, pressure, and temperature) coupled with Parrinello–Rahman pressure was used.[25] Production MD was carried out for 150 ns, and the coordinates were saved for further analysis.

PCA and FEL Analysis. The energy profile of proteins through their trajectories can be obtained from principle component analysis (PCA).[26] The cosine content (ci) of the principal component (pi) of the covariance matrix was defined by atomic fluctuations of the dihedral angles (Φ, Ψ) of the protein molecule during simulation. The free energy landscape (FEL) derived from PCA denotes intervals from the trajectories and was selected by the cosine content value. Generally, the values of cosine content range from 0 to 1 for simulation time. The value near 1 exhibits the larger motion whereas values between 0.2 and 0.5 represent smooth and single basin.[27]

$$Ci = \frac{2}{T}\left(\int \cos(i\pi t) Pi(t)dt\right)^2 \left(\int Pi^2(t)dt\right)^{-1}$$

The eigenvectors of the docked β-β'-PUM complex were generated, and their cosine content values were analyzed. The PCs having cosine content values less than 0.2 were chosen for the FEL and used to select the models with favorable interaction.

Binding Energies. The energy contribution and binding free energy (ΔG_{bind}) contribution of the protein-ligand complex were calculated using the GROMACS tool g_mmpbsa, which is based on the molecular mechanics Poisson–Boltzmann surface area (MM-PBSA) method.[28] The binding free energy is calculated using the following equation,

$$\Delta G_{bind} = E_{MM} + G_{solv} - T\Delta S$$
$$= E_{vdw} + E_{elec} + G_{polar} + G_{nonpolar} - T\Delta S$$

where $T\Delta S$ is the conformational entropy at temperature T, ΔG_{solv} denotes the solvation free energy, which includes nonpolar ($G_{nonpolar}$) and polar (G_{polar}) contributions, and E_{MM} represents the molecular mechanics of the free energy in the gas phase, including the van der Waals (E_{vdW}) and electrostatic (E_{elec}) contributions. The energy components were calculated using the 10 snapshots extracted from 75 to 150 ns of the production MD trajectory of the β-β'-PUM complex. The energy decomposition method was employed between the protein and the ligand for calculation of the interaction energy. The E_{MM} was used to determine the binding interaction in the complex.

Cloning Expression and Purification of the β' N-Terminal Domain. The *rpoC* gene (RpoC, accession no.: NP_268496.1) coding for N-terminal residues Phe7-Asp818 was amplified by polymerase chain reaction (PCR) from the genomic DNA of the *S. pyogenes* M1 strain (MTCC) and cloned in the pEC-K-HT-HIS (2) in-house vector at EcoR1 and BamH1 sites. The construct was transformed into the expression host BL21 (DE3) strain of *Escherichia coli*. For protein expression, the transformed *E. coli* cells were cultured in Luria–Bertani (LB) medium. An overnight culture (10 mL) was prepared and transferred to 1 L of LB medium supplemented with 50 mg/mL kanamycin. The culture was grown at 37 °C at 150 rpm shaking until the desired optical density of 0.6 at A_{600} was obtained. The culture was induced with 1 mM isopropyl β-D-1-thiogalactopyranoside (IPTG) for protein expression and incubated further for 4 h with shaking. The cells were harvested by centrifugation at 4000 rpm for 20 min at 4 °C. The cell pellet was suspended in lysis buffer containing 20 mM Tris pH 7.0, 300 mM NaCl, and 10% glycerol, and the cells were lysed by sonication on ice. The cell lysate was centrifuged at 10,000 rpm for 45 min at 4 °C, and the pellet was used for purification.

The protein was solubilized from the pellet using buffer containing 20 mM Tris pH 7.0, 300 mM NaCl, 10% glycerol, and 10% *N*-lauroylsarcosine by continuous stirring at 150 rpm for 1 h at 4 °C and centrifuged at 10,000 rpm for 30 min at 4 °C. The solubilized protein was further refolded by stepwise membrane dialysis against lysis buffer containing 5, 2.5, 1, and 0% *N*-lauroylsarcosine, respectively, for 3 h at 4 °C. As the protein was expressed with an N-terminal His-tag, purification was carried out by nickel-affinity chromatography. At each step, the purity of the fractions was analyzed on a 10% SDS-PAGE gel. The concentration of protein was measured using a UV spectrophotometer (A_{280}) and presumed calculated absorption coefficient of 0.789 from the PROTPARAM online tool.[29]

Isothermal Titration Calorimetry. Isothermal titration calorimetry (ITC) using a Nano-ITC (TA Instruments-Waters, New Castle, DE, USA) was performed to analyze the interaction of protein with PUM. The buffers used for preparation of protein and ligand samples were degassed systematically to remove air bubbles. Purified protein (10 μM) was dialyzed for 16 h at 4 °C against 20 mM Tris pH 7.0 and 20 mM NaCl and was taken in the sample cell. The PUM ligand (obtained from Med Chem Express LLC) prepared in the same buffer was injected in small volumes (2 μL) at equal intervals (300 s) into the sample cell in a series of 25 injections. The experiment was conducted at 25 °C with the stirrer at the constant speed of 309 rpm. The integrated heat data was investigated in an independent model by nonlinear least-squares minimization fitting using NanoAnalyze (TA Instruments), and the thermodynamic factors enthalpy change (ΔH), change in entropy (ΔS), association constant (K_a), dissociation constant (K_d), and free energy change (ΔG) were calculated.

Circular Dichorism (CD) Spectroscopy. The far-UV (190–250 nm) and near-UV (250–350 nm) spectra for refolded protein and protein-PUM complex were recorded on the JASCO J-815 spectrophotometer using 0.1 and 1 cm path length cuvettes, respectively. The concentration of protein was kept at 20 μM in 20 mM phosphate buffer pH 7.4; protein and the ligand were incubated in the molar ratios 1:1, 1:5, and 1:10, respectively, for 30 min. The baseline correction was performed using phosphate buffer, and the data was converted to mean delta epsilon θ, in mdeg·cm^2·dmol^{-1}. The secondary structural details of the protein alone and the protein-ligand complex were analyzed using the K2D2 online tool.[30] The protein secondary structure prediction based on sequence was carried out using the Self Optimized Prediction Method with Alignment (SOPMA)[31] tool.

Intrinsic Fluorescence Quenching. Intrinsic fluorescence spectra of the protein and protein-ligand complex were recorded on a SpectroMax M2e multimode reader using a 96-well microtitration plate. All measurements were taken at four different temperatures: 24 °C, 27 °C, 30 °C, and 33 °C. The concentration of protein was kept constant at 1 mM in each well, and PUM was added in increasing concentration from 0.1 to 0.9 mM. Intrinsic fluorescence was scanned at an excitation

https://doi.org/10.1021/acsomega.2c07805
ACS Omega 2023, 8, 7989–8000

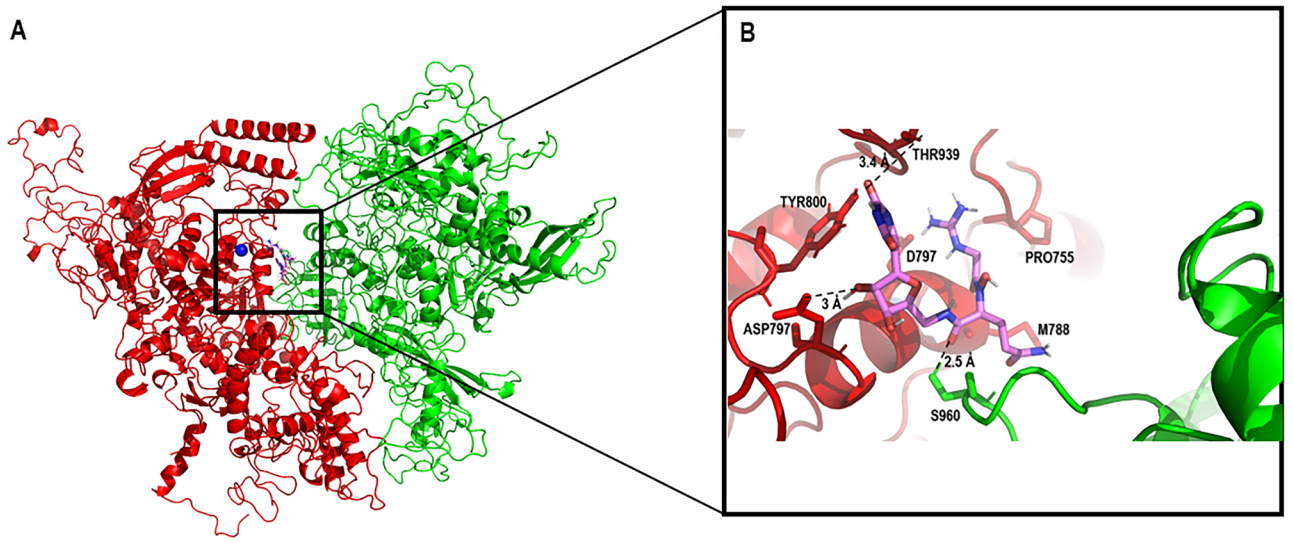

Figure 2. (A) Molecular docked structure of the RNA polymerase β subunit (RpoB—green), β' subunit (RpoC—red), and pseudouridimycin (PUM—pink); Mg^{2+} ion is shown as a blue sphere. (B) Close-up view of the residues of the β and β' subunits interacting with PUM. Hydrogen bonds are shown in dotted lines.

wavelength of 280 nm and an emission wavelength in the 300−500 nm range. The excitation and emission bandwidth slits were set to 5 nm.[32] Experiments were repeated in triplicate, and suitable blanks without PUM corresponding to buffer and protein were used as control. The fluorescence quenching titration results were examined for the quenching mechanism involved in the protein-PUM interaction with the aid of the Stern−Volmer equation:

$$F_0/F = 1 + K_{SV}[D] = 1 + K_q\tau_0[D]$$

where F_0 is the intensity of protein alone and F is the intensity of fluorescence after the addition of PUM; K_{SV} is the quenching constant; K_q is the quenching rate constant; $[D]$ is the concentration of PUM; and τ_0 is the average lifetime of Trp and Tyr residues in protein without PUM.

RESULTS AND DISCUSSION

Minimum Inhibitory Concentration. One of the simplest techniques for determining antimicrobial susceptibility is the broth microdilution method. Pseudouridimycin, a microbial nucleoside analogue inhibitor, was reported as a lead compound targeting RNA polymerase complex in some drug-resistant bacterial species.[15] Though PUM was shown to be effective against both Gram-positive and Gram-negative strains, further study was carried out to ascertain its efficacy on demographically different strains. The antibacterial activity of PUM against erythromycin-resistant clinical strains of *S. pyogenes* was evaluated. Two clinical samples, characterized as erythromycin resistant and a standard MTCC strain, were employed for the PUM sensitivity assay. The antimicrobial agent PUM (initial stock—1 mg/mL) was diluted in sterile water and dispensed in a 96-well microtitration plate with sterile MHB medium (100 μL). Each well was inoculated with *S. pyogenes* inoculum prepared in MHB medium. For erythromycin-resistant clinical strains, the MIC values obtained were in the range of 0.1−1 μg/mL, which was greater than the reported concentration 2−12 μg/mL (Figure S1).[15] The MIC results were in concordance with earlier reports, showing that PUM is able to inhibit erythromycin-resistant strains of *S. pyogenes*.[15]

Molecular Docking between β-β' Protein Complexes with PUM Ligand. Considering the potential antibacterial activity of PUM against macrolide-resistant strains of *S. pyogenes* and based on previous studies of PUM in *T. thermophilus*, the RNA polymerase subunits β and β' of GAS were chosen as possible targets of our study. Three-dimensional structural models of the RNA polymerase complex composed of the major subunits (encoded by *rpoB* and *rpoC* genes) were generated. Molecular docking was performed to understand the precise mechanism of the interaction of PUM with the β-β' complex. Earlier studies have reported PUM binding to the NTP addition site the of *T. thermophilus* RNA polymerase complex.[15] Consequently, in GAS, PUM binding sites were predicted by sequence comparison (Figures S2 and S3) and induced fit docking methods. The binding pocket consisted of residues from both subunits: Glu525 and Lys928 from β subunit and Arg415, Asn448, Gly787, Thr791, and Gln934 from the β' subunit. The key moiety of PUM, namely glutamine amide, interacts with the β subunit while the guanidinyl terminus and 6′ amino pseudouridine interact with the β' subunit (Figure 1). The docked complex was stabilized by nine hydrogen bonds showing key interactions with the Tyr800 residue and sixty-four nonbonded contacts (Figure 2). The binding energy ΔG *-64.38 kJ/mol*, docking score −10.11, and glide energy score −64.84 kcal/mol of the docked complex were calculated (Table 1).

Molecular Dynamics Simulation of the β-β'-PUM Complex. The stability of the RNAP β-β'-PUM complex was further examined using MD simulations. The protein complex and protein-ligand complex were subjected to 150 ns simulation. The RMSD profiles for the protein (apo form) and protein-ligand complex showed a deviation ranging from 0.5 to 1.5 nm without a major drastic change throughout the simulation. The individual chain (β and β') analysis for both the apo form and the ligand-bound form showed deviations in the range of 4−7 nm. The apo form showed rms deviations in the range of 4−7 nm while the ligand-bound complex was stable with deviations in the 5−6 nm range illustrating the stabilization of protein complex after binding with ligand

https://doi.org/10.1021/acsomega.2c07805
ACS Omega 2023, 8, 7989−8000

Table 1. Hydrogen Bond Interaction of Docked β′-β-PUM Complex Analyzed Using the PDB-Sum Server

s.no.	RpoC-RpoB	PUM	hydrogen bond distance (Å)
1	B: ASP 797[OD1]	LIG [O3]	2.60
2	B: MET 788[O]	LIG [N5]	3.10
3	B: ASP 790[OD1]	LIG [N7]	2.98
4	B: TYR 800[OH]	LIG [O7]	3.08
5	B: THR 939[OG1]	LIG [O7]	3.00
6	B: PRO 755[O]	LIG [N8]	2.89
7	B: ASP 790[OD1]	LIG [N8]	2.75
8	A: SER 960[N]	LIG [O9]	2.92

(Figure 3). Throughout the simulations, PUM remained in the binding pocket and FEL analysis was performed to obtain the lowest energy structure (depicted in dark blue in Figure 4). Protein-ligand interactions were investigated for all 38 structures obtained from the cluster. Analysis of a representative structure from the cluster at 120 ns showed PUM forming five hydrogen bonds: two with Ser960 from the β subunit, two with Tyr800, and one with Phe940 from the β′ subunit (Table 2). The interactions of the critical residue Tyr800 of the β′ subunit were maintained throughout the simulations, depicting its major role in complex formation (Figure 5).

The molecular mechanics energies applied to the protein-ligand complex have led us to estimate the free energy of ligand binding at the cavity of the protein. It emphasizes the ligand binding affinities over the simulation time along with the solvent accessibility. The dynamic studies along with MM/GBSA results provide insight into the PUM ligand interaction. The overall values of the electrostatic and van der Waals energies are −0.710 kJ/mol and −206.108 kJ/mol, respectively. The uncertainty in the protonation of protein holds the polar solvation energy to be in the range of 89.654 kJ/mol. The solvent-accessible surface area energy of the complex is −18.658 kJ/mol, indicating the magnitude of its ligand affinity toward the protein. From the simulations, the free ligand interacts with the protein with an overall binding energy ΔG_{bind} of −135.821 ± 17.111 kJ/mol, demonstrating favorable binding affinity (Table 3). The protein-ligand complex interaction pattern and energy analysis revealed that PUM remained intact in the binding region and was stabilized via hydrogen bonds. Interestingly, the binding environment of PUM in the complex is comprised of Tyr800 and Phe940 residues of the β′ subunit around 5 Å distance before and after MD simulations and has been characterized further through spectroscopic studies.

Protein-PUM Interaction Analysis by ITC. Understanding the physicochemical mechanics behind the interaction between a protein and ligand is crucial to comprehend the molecular recognition between them. The thermodynamic properties involved in molecular interactions such as K_a, K_d, ΔS, ΔH, and n were calculated from ITC. The real-time interaction of protein-ligand complex formation was assessed from the thermodynamic signature for the N-terminal domain of the β′ subunit with PUM. The N-terminal domain of the β′ subunit was chosen based on the location of the highly conserved catalytic active center (NADFDGD)[17] where PUM binding was identified (Figures 6 and 7). In Figure 8 the upper panel shows the heat released during the titration of 2 μL of 100 μM PUM into 10 μM protein in 25 injections. The lower panel (Figure 8) depicts the curve fitting using an independent model of binding to the protein and its corresponding thermodynamics parameters.

In a thermodynamic system, enthalpy is determined by adding the internal energies of its solute and solvent as well as the energy needed to create space for them. The binding enthalpy is typically the change in energy brought on by the formation of noncovalent interactions at the binding interface, such as van der Waals contacts, hydrogen bonds, ion pairs, and any other polar and apolar interactions.[33] The ΔH value obtained was −524 kJ/mol, demonstrating an exothermic process. The entropy (ΔS) system is a thermodynamic attribute, with positive and negative values denoting an overall increase or decrease in the degree of freedom. In our experiment, a negative value of −1648 J/mol·K during the protein-PUM interaction implies a decrease in the disorder of the system, promoting tight binding of PUM to protein. Numerous favorable noncovalent interactions result in tight binding between association partners with a significant negative enthalpy change. Subsequently, this change was accompanied by negative entropy due to the restricted mobility of interacting partners, as evidenced by a marginal change in the binding free energy.[34] Interestingly, it was noted

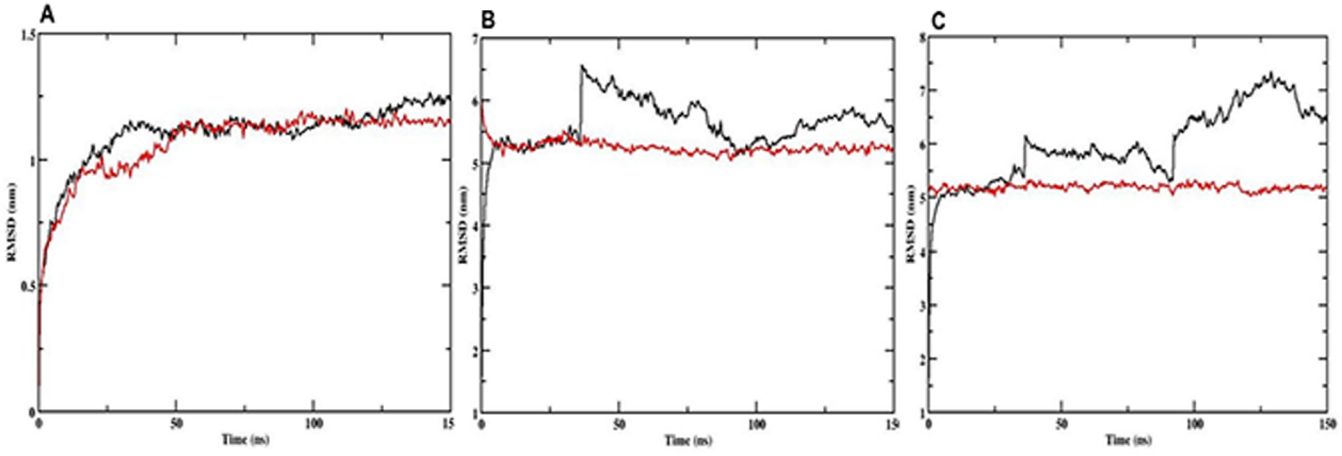

Figure 3. RMSD profile of 150 ns production MD of the β-β′-PUM complex. (A) Overall RMSD regions of the β-β′ complex with PUM (red) and without PUM (black). (B) RMSD profile of the β subunit with PUM (red) and without PUM (black). (C) RMSD profile of the RpoC chain with PUM (red) and without PUM (black).

https://doi.org/10.1021/acsomega.2c07805
ACS Omega 2023, 8, 7989−8000

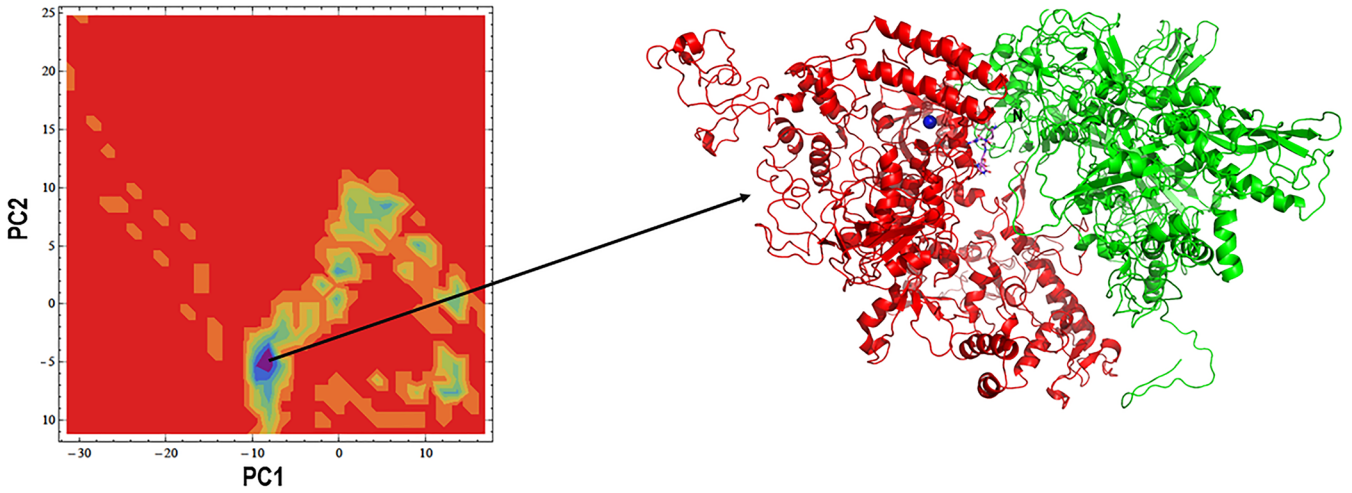

Figure 4. Free energy landscape (FEL) analysis used to retrieve the lowest energy structure during the MD simulation. The dark blue cluster indicates a collection of lowest energy structures. From this cluster, the complex with lowest energy and favorable interactions was chosen for analysis. The RNA polymerase β subunit (RpoB—green), β' subunit (RpoC—red), and pseudouridimycin (PUM—pink) are shown.

Table 2. Hydrogen Bond Interaction of the Lowest Energy Structure of the β'-β-PUM Complex Obtained from FEL Analysis

s.no.	RpoC-RpoB	PUM	hydrogen bond distance (Å)
1	A: SER 960[N]	LIG [O9]	3.00
2	A: SER 960[OG]	LIG [O5]	2.55
3	B: TYR 800[OH]	LIG [O7]	2.97
4	B: TYR 800[OH]	LIG [N3]	2.88
5	B: PHE 940[N]	LIG [O7]	3.31

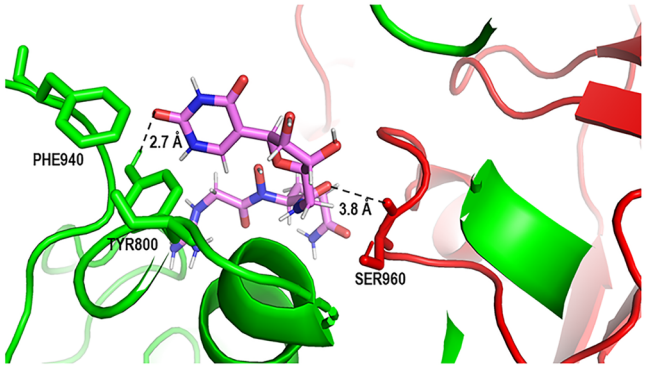

Figure 5. Protein-ligand interaction of the lowest energy docked complex obtained from FEL analysis. The active site residues involved interaction of the RNA polymerase β subunit (RpoB—green), β' subunit (RpoC—red), and pseudouridimycin (PUM—pink).

Table 3. MM-GBSA Calculation for the β'-β-PUM Complex Obtained from Molecular Dynamics Simulation

S.No.	MM-GBSA calculation	
1	van der Waal energy	−206.108 ± 15.878 kJ mol^{-1}
2	electrostatic energy	−0.710 ± 23.402 kJ mol^{-1}
3	polar solvation energy	89.654 ± 19.344 kJ mol^{-1}
4	SASA energy	−18.658 ± 1.100 kJ mol^{-1}
5	binding energy	−135.821 ± 17.111 kJ mol^{-1}

that both the enthalpy and entropy changes were negative, and upon closer inspection, it is evident that the entropy contribution was two times lesser than the enthalpy change.

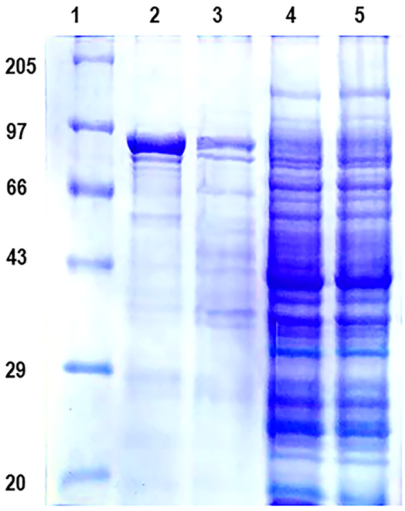

Figure 6. 10% SDS/PAGE gel showing expression of the RpoC N-terminal construct. Lanes: **1**, broad range molecular weight ladder (kDa); **2**, pellet fraction induced with 1 mM IPTG; **3**, supernatant fraction induced with 1 mM IPTG; **4**, uninduced supernatant; and **5**, uninduced pellet fraction.

Protein-ligand binding, like any spontaneous process, happens only when the change in the system's Gibbs free energy ΔG is negative where the system reaches an equilibrium state under constant pressure and temperature.[35] The overall free energy was −33.05 kJ/mol, which determines the stability of the protein-ligand complex and represents the reaction as a spontaneous process.

The association constant between protein and PUM interaction was calculated as 6.175×10^5 M^{-1}, denoting a moderate affinity. Hence this affinity would eventually induce a faster diffusion of ligand to reach the target site.[36] The number of binding sites of PUM on the protein was observed as 1.1 (Table 4). PUM binding is therefore enthalpy-driven, and noncovalent interactions such as van der Waals forces and hydrogen bonds stabilize the binding.

Circular Dichroism Spectroscopy of Protein and Ligand. The secondary structure and conformational changes in the protein upon PUM binding were evaluated using CD

https://doi.org/10.1021/acsomega.2c07805
ACS Omega 2023, 8, 7989−8000

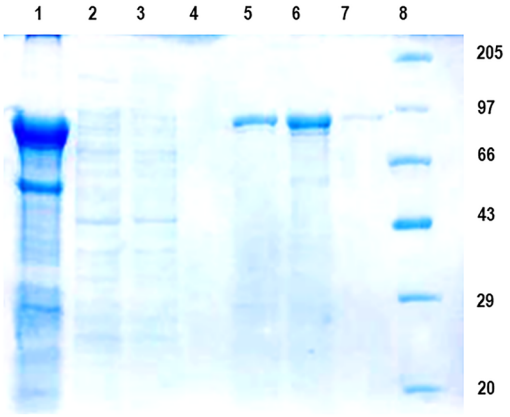

Figure 7. 10% SDS/PAGE gel showing purification of the RpoC N-terminal construct. Lanes: **1**, induced supernatant; **2**, flow through; **3**, buffer wash with 10 mM imidazole; **4**, buffer with 100 mM imidazole; **5**, buffer with 200 mM imidazole; **6**, buffer with 300 mM imidazole; **7**, buffer with 400 mM imidazole; **8**, broad range molecular weight ladder (kDa). Elutions seen in lanes **5** and **6** were chosen for further studies.

spectroscopy. The CD spectra of the protein and protein with PUM at 190−250 nm reveal no notable structural changes upon ligand binding. The CD spectrum of the protein showed two negative bands in the UV region between 208 and 222 nm, which were caused by the n-π* transition[37] (Figure 9). A gradual decrease in band intensity was observed with the addition of PUM in various molar ratios without any appreciable change in peak positions. The percentage of secondary structures was computed from the CD results using the K2D2 web server. CD data showed the protein contains 39% helices and 11% sheet (Table 5). The helicity percentage

Table 4. Thermodynamic Parameters Obtained by ITC Experiments for Protein with PUM

S.No.		ITC
1	K_d	1.620×10^{-6} M
2	n	1.167
3	ΔH	−524.5 kJ mol^{-1}
4	ΔS	−1648 J/ mol^{-1} K^{-1}
5	ΔG	−33.05 kJ mol^{-1}
6	$-T\Delta S$	491.4
7	K_a	6.175×10^{5} M^{-1}

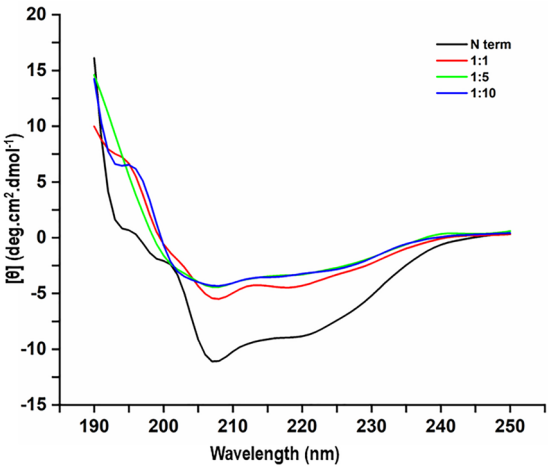

Figure 9. Far-UV CD spectra of protein with various molar concentrations of PUM. The graphs of protein alone (black) and protein:PUM in 1:1 (red), 1:5 (green), and 1:10 (blue) ratios are depicted.

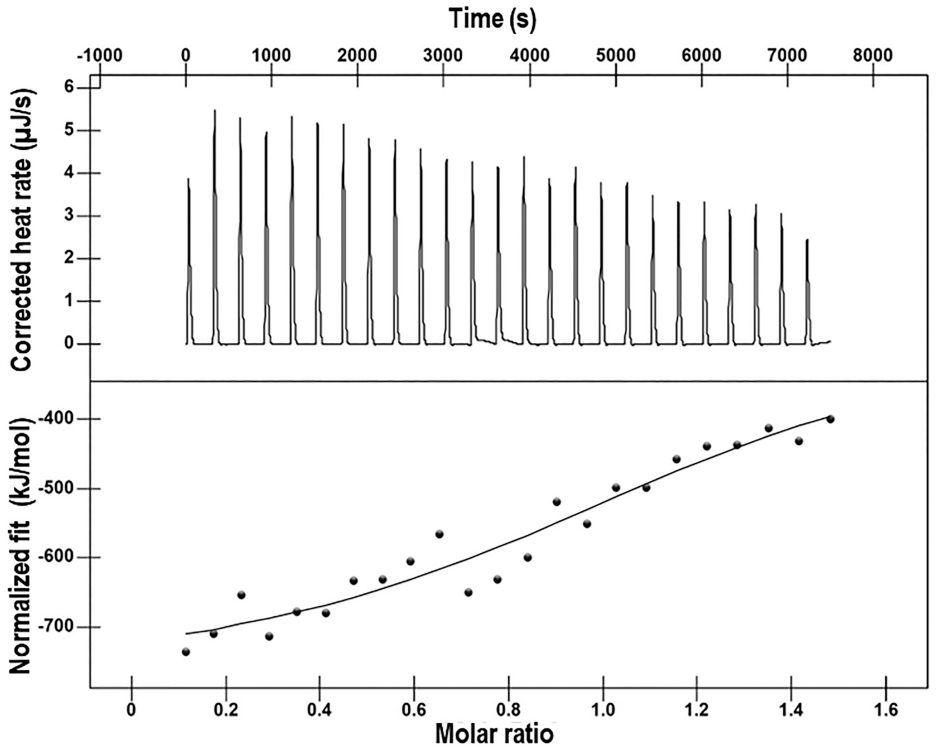

Figure 8. Isothermal titration calorimetry thermogram of protein (15 μM) against PUM (100 μM). The upper panel shows the raw thermogram data, and the lower panel indicates the isotherm obtained by the plot of integrated heat versus protein/ligand molar ratio.

https://doi.org/10.1021/acsomega.2c07805
ACS Omega 2023, 8, 7989−8000

Table 5. CD Analysis by Using SOPMA and the K2D2 Server for the Protein-PUM Complex

	α-helix%	β-sheet%
CD Prediction Using K2D2 Server		
protein	39.37	11.52
protein + PUM (1:1)	40.18	10.65
protein + PUM (1:5)	37.03	11.69
protein + PUM (1:10)	37.03	11.69
Sequence Prediction Using SOPMA		
protein	44.33	17.0

continuously fluctuated between 40 and 37% with the addition of PUM at molar ratios of 1:1, 1:5, and 1:10, whereas the sheet conformation remained unchanged and maintained in the range of 10−11%. Therefore, this data indicates that addition of PUM to protein did not alter the secondary structure significantly.

The microenvironment of aromatic amino acid side chains and disulfide bonds contributes to the near-UV CD of proteins. Each aromatic amino acid typically has a distinctive wavelength signature; tyrosine has a peak between 275 and 282 nm, whereas tryptophan has a peak between 290 and 305 nm. A sharp reasonable peak of phenylalanine was observed between the wavelengths 255 and 270 nm.[38] The occurrence of maxima around 255−280 nm in the near-UV CD spectra of protein was attributed to the presence of aromatic amino acid phenylalanine and tyrosine residues (Figure 10).[39] Addition of

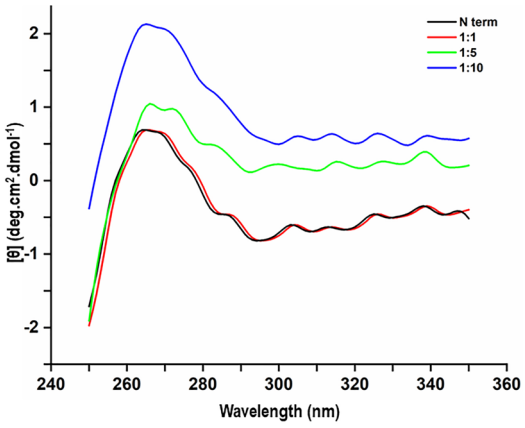

Figure 10. Near-UV CD spectra of protein with various molar concentrations of PUM. The graphs of protein alone (black) and protein:PUM in 1:1 (red), 1:5 (green), and 1:10 (blue) ratios are depicted.

PUM at increasing concentrations clearly increases the peak intensity, indicating a potential interaction with protein. From the CD, it is deciphered that PUM binding does not alter the secondary structural integrity but affects the local tertiary structure of the Tyr and Trp aromatic side-chain residues significantly.

Intrinsic Fluorescence Quenching of Protein. A sensitive technique for examining the binding interaction of small molecules with proteins is fluorescence quenching measurement. Intrinsic fluorophores are naturally present in proteins and undergo quenching when they form a complex with ligand. Fluorophores in the excited state collide with quenchers in a molecular process to cause dynamic quenching while static quenching, on the other hand, is triggered by development of a ground-state combination of fluorophores and quenchers.[40] The fluorescence lifetime and its dependence on temperature change distinguish dynamic and static quenching constants.[41] Higher temperatures result in a larger diffusion coefficient, which causes the dynamic quenching constant to rise with temperature. In contrast, the static quenching constant decreases with increasing temperature because the complex becomes less stable.[42] The fluorescence spectra of protein-PUM at different temperatures were measured to identify the varying tendency of the quenching constant (K_{sv}). The fluorescence emission spectrum of protein and protein with PUM at various concentrations ranging from 100 to 900 μM with 100 μM intervals was measured. The protein emission spectrum showed a maximum emission peak at 320 nm, which was attributed to the presence of 23 tyrosine residues.[43] The decrease in the protein fluorescence intensity in the presence of PUM indicates protein-ligand interaction. The observed quenching in protein fluorescence could be attributed to various molecular interactions like collisional quenching, energy transfer, complex formation of either ground state or excited state, and reorganization of molecules[44] (Figures 11, 12, 13, and 14).

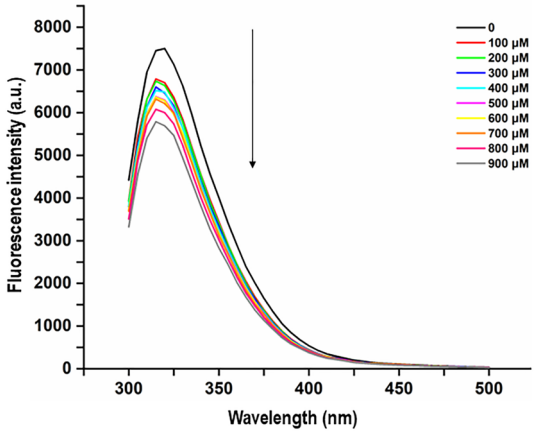

Figure 11. Steady state emission spectra of protein (1 mM) with PUM concentrations ranging from 100 μM to 900 μM at 24 °C. The graph in black indicates protein, and other colors depict protein with varying concentrations of PUM.

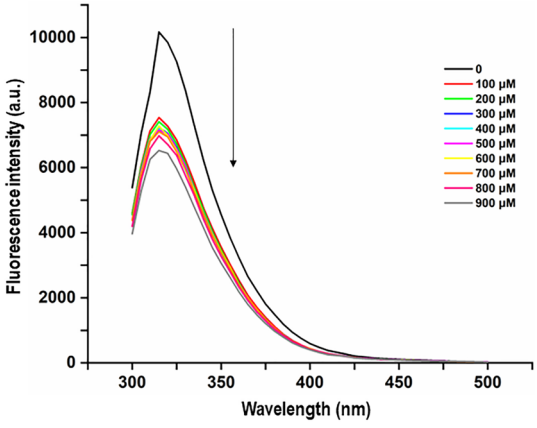

Figure 12. Steady state emission spectra of protein (1 mM) with PUM concentrations ranging from 100 μM to 900 μM at 27 °C. The graph in black indicates protein, and other colors depict protein with varying concentrations of PUM.

https://doi.org/10.1021/acsomega.2c07805
ACS Omega 2023, 8, 7989−8000

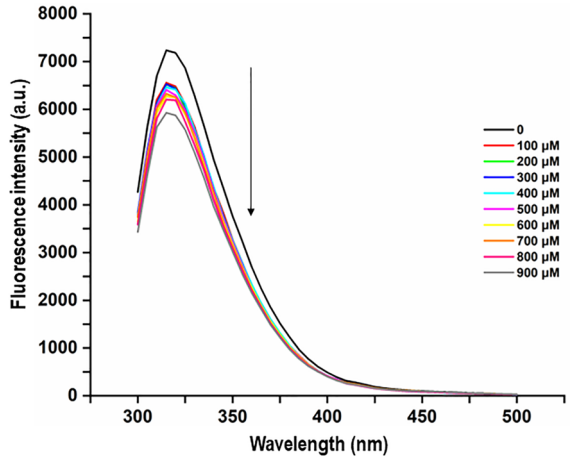

Figure 13. Steady state emission spectra of protein (1 mM) with PUM concentrations ranging from 100 μM to 900 μM at 30 °C. The graph in black indicates protein, and other colors depict protein with varying concentrations of PUM.

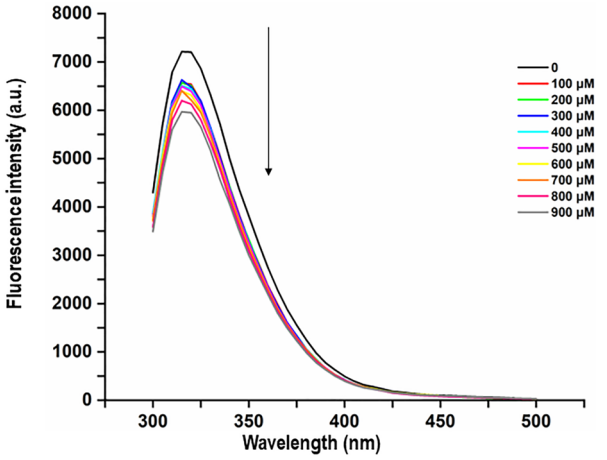

Figure 14. Steady state emission spectra of protein (1 mM) with PUM concentrations ranging from 100 μM to 900 μM at 33 °C. The graph in black indicates protein, and other colors depict protein with varying concentrations of PUM.

The Stern−Volmer equation was used to analyze the quenching mechanism involved in the protein-PUM interaction at four temperatures: 24 °C, 27 °C, 30 °C, and 33 °C. The quenching constant K_{sv} was obtained for all four temperatures using linear fit (Figure 15). From the values (Table 6), it is inferred that K_{sv} values decrease with an increase in temperature, indicating static quenching rather than dynamic quenching, forming a stable complex.[44] Furthermore, the calculated biomolecular quenching constant was in the order of 10^{14} for four different temperatures, which is higher than the maximum dynamic collisional quenching constant of 2.0×10^{10} L mol−1 s^{-1}, which affirms the interaction between protein and PUM. These findings resoundingly support the theory that static collisions cause quenching and result in the formation of a complex between protein and PUM.

Implication of PUM Interaction with Protein. Analysis of the interacting pattern of the protein-ligand complex through molecular dynamics showed that PUM remained intact within the binding regions, stabilized by hydrogen bonds. A close inspection of the binding environment reveals the presence of aromatic amino acid Phe328, Phe940, and

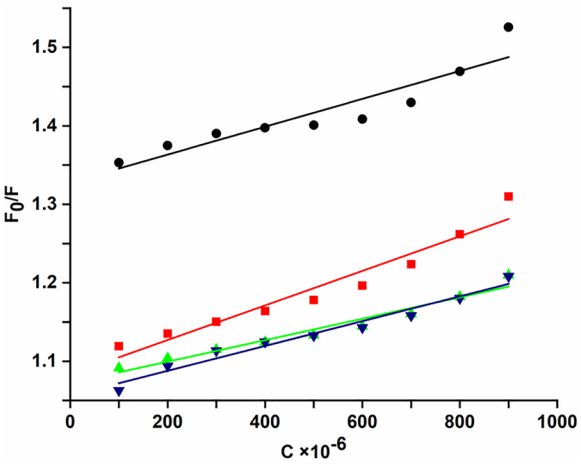

Figure 15. Stern−Volmer plots for protein with PUM ligand at different temperatures, namely 24 °C (red), 27 °C (black), 30 °C (green), and 33 °C (blue).

Table 6. Quenching Constant and Biomolecular Quenching Rate Constant Determined by Intrinsic Fluorescence for the Protein-PUM Complex

T (K)	K_{sv} (×10^4 L/mol)	K_q (×10^{14} L mol^{-1} s^{-1})
298	2.20	5.66
301	1.78	4.57
304	1.37	3.51
307	1.37	3.51

Tyr800 residues of the β' subunit at a distance of 6 Å, before and after MD simulation (Figure 16). The binding environment of PUM in the protein-ligand complex was further ascertained by the intrinsic aromatic amino acid signals using other biophysical techniques. The CD measurements in the near-UV absorption spectrum shed light on the tertiary structural change of the complex, as the peaks obtained corresponded to phenylalanine and tyrosine residues present in the protein (Figure 17). The changes in the absorbance upon PUM addition clearly indicate micro environmental alterations around protein chromophores due to protein-PUM complex formation. Further, the quenching mechanism of the tyrosine residues in the binding environment of PUM was investigated by the intrinsic fluorescence signal of the protein, which was quenched by addition of PUM. The experimental results were comparable to the MD studies, which highlight the fact that PUM binds to a hydrophobic pocket comprised of Phe and Tyr residues. The overall binding free energy of the complex was higher along with the van der Waal energy which favored tight association of PUM toward the protein throughout the simulation. Concurrently, the thermodynamic parameters by ITC show that the major contribution of complex formation was favored by noncovalent interactions, van der Waals forces, and hydrogen bonds. Hence these results illustrate the importance of phenylalanine and tyrosine residues and stabilization of the complex by hydrogen bonds and van der Waals forces.

CONCLUSION

In this work, the interaction of the RNA polymerase β' subunit of GAS with pseudouridimycin, a nucleotide analogue inhibitor, has been characterized using spectroscopy, calorimetry, and computational studies. Previous studies have reported

https://doi.org/10.1021/acsomega.2c07805
ACS Omega 2023, 8, 7989−8000

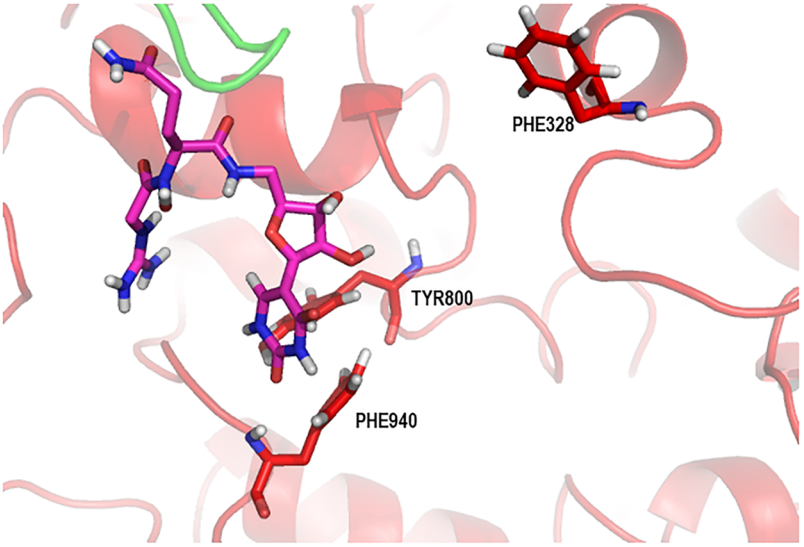

Figure 16. Presence of tyrosine and phenylalanine residues around 6 Å from PUM in the protein ligand complex (RpoB—green), β' subunit (RpoC—red), and pseudouridimycin (PUM—pink).

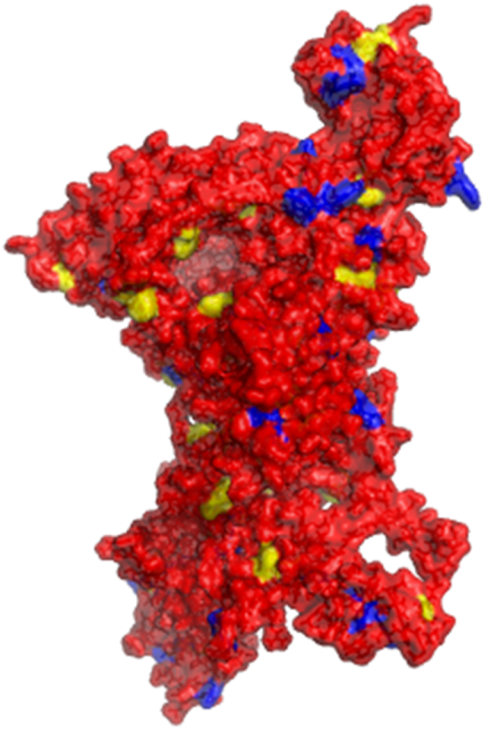

Figure 17. Surface representation of the β' subunit (red) where phenylalanine residues are highlighted in yellow and tyrosine residues are shown in blue.

PUM as a lead compound for drug-resistant bacteria targeting the RNA polymerase complex. In our study, PUM was tested against erythromycin-resistant *S. pyogenes* clinical strains for its antibacterial efficacy. The MIC values were obtained in the range of 0.1−1 μg/mL concentration, which was higher compared to the already reported efficacy of approximately 2−12 μg/mL. Subsequently, the three-dimensional structural models of the RNA polymerase β and β' complex were docked with PUM compound at the NTP addition site, and further stability of the complex was assessed through MD simulations. Although the overall RMSD profile of the apo form and the docked complex failed to show any notable difference, the individual chain fluctuations were higher in the apo form when compared to the protein-ligand complex. Experimentally, the real-time interaction of protein-ligand formation and their thermodynamic signature was studied by ITC for the N terminal domain of the β' subunit with PUM. The result shows that complex formation was predominantly enthalpy driven, exothermic, and spontaneous in nature. These parameters emphasize that the protein-PUM complex was evidently stabilized by hydrogen bonds and van der Waals interactions as reported in MD studies. Further insights into PUM-protein interaction were deciphered from clues obtained from the binding environment of the complex by exploiting the intrinsic aromatic amino acid signal using CD and intrinsic fluorescence quenching. The aromatic amino acids Tyr800 and Phe940 play an important role in complex formation, and their interactions were evident, as confirmed by our computational studies and spectroscopic experiments. Apart from the noncovalent interactions, hydrophobic interactions are crucial in capturing PUM in the binding cavity, thus forming a steady complex. A strong conclusion can be drawn from the combined findings that PUM is a powerful inhibitor of the RNA polymerase complex of *S. pyogenes* pathogen and can be used as a novel inhibitor for macrolide-resistant strains.

■ ASSOCIATED CONTENT

Supporting Information

The Supporting Information is available free of charge at https://pubs.acs.org/doi/10.1021/acsomega.2c07805.

Minimum inhibitory concentration assay of macrolide resistant clinical strains and MTCC strain of *S. pyogenes*; and multiple sequence alignment of the β-subunits and β'-subunits of *S. pyogenes* and *T. thermophilus* (PDF)

■ AUTHOR INFORMATION

Corresponding Author

Preethi Ragunathan − *Centre of Advanced Study in Crystallography and Biophysics, University of Madras, Chennai 600 025, India;* orcid.org/0000-0003-0221-9252; Email: preeth_182003@yahoo.co.in

https://doi.org/10.1021/acsomega.2c07805
ACS Omega 2023, 8, 7989−8000

Authors

Kunthavai Pavundurai Chandra − *Centre of Advanced Study in Crystallography and Biophysics, University of Madras, Chennai 600 025, India*

Damodharan Perumal − *Department of Microbiology, Dr ALM PGIBMS, University of Madras, Chennai 600 113, India*

Complete contact information is available at: https://pubs.acs.org/10.1021/acsomega.2c07805

Author Contributions

P.R. and K.P.C. designed the experiments. K.P.C. conducted the experiments. D.P performed the microbial assay. P.R. and K.P.C. wrote the manuscript and Supporting Information.

Notes

The authors declare no competing financial interest.

■ ACKNOWLEDGMENTS

The authors thank The Council of Scientific & Industrial Research (CSIR)-Senior Research Fellowship (SRF) (09/115(0798)/2020 EMR-I, dt. 15th March 2021), New Delhi, for providing the financial support to carry out this work. P.R. thanks DST-FIST, Government of India for the computational facilities sanctioned to the department (No: SR/FST/LSII-037/2014 (C) dt. 29.03.2016). P.R. would like to thank SERB for the EMR funding support. The authors thank Dr. Aruna Ganesan, Department of Medical Physics, Anna University Chennai, for the fluorescence studies and Dr. D. Prabhu, Department of Medical Microbiology, University of Madras, for the antibacterial assays.

■ REFERENCES

(1) Cunningham, M. W. Pathogenesis of group A streptococcal infections. *Clin Microbiol Rev.* **2000**, *13* (3), 470−511.

(2) Chan, K. H.; Veeraballi, S.; Ahmed, E.; Yakobi, R.; Slim, J. A Case of Co-occurrence of COVID-19 and Group A Streptococcal Pharyngitis. *Cureus* **2021**, *13* (4), No. e14729.

(3) Brown, E. D.; Wright, G. D. Antibacterial drug discovery in the resistance era. *Nature* **2016**, *529* (7586), 336−43.

(4) Chellat, M. F.; Raguz, L.; Riedl, R. Targeting Antibiotic Resistance. *Angew. Chem., Int. Ed. Engl.* **2016**, *55* (23), 6600−26.

(5) Artsimovitch, I.; Vassylyeva, M. N.; Svetlov, D.; Svetlov, V.; Perederina, A.; Igarashi, N.; Matsugaki, N.; Wakatsuki, S.; Tahirov, T. H.; Vassylyev, D. G. Allosteric modulation of the RNA polymerase catalytic reaction is an essential component of transcription control by rifamycins. *Cell* **2005**, *122* (3), 351−63.

(6) McClure, W. R. On the mechanism of streptolydigin inhibition of Escherichia coli RNA polymerase. *J. Biol. Chem.* **1980**, *255* (4), 1610−6.

(7) Sergio, S.; Pirali, G.; White, R.; Parenti, F. Lipiarmycin, a new antibiotic from Actinoplanes III. Mechanism of action. *J. Antibiot (Tokyo)* **1975**, *28* (7), 543−9.

(8) Zhang, Y.; Degen, D.; Ho, M. X.; Sineva, E.; Ebright, K. Y.; Ebright, Y. W.; Mekler, V.; Vahedian-Movahed, H.; Feng, Y.; Yin, R.; Tuske, S.; Irschik, H.; Jansen, R.; Maffioli, S.; Donadio, S.; Arnold, E.; Ebright, R. H. GE23077 binds to the RNA polymerase 'i' and 'i+1' sites and prevents the binding of initiating nucleotides. *Elife* **2014**, *3*, No. e02450.

(9) Mukhopadhyay, J.; Das, K.; Ismail, S.; Koppstein, D.; Jang, M.; Hudson, B.; Sarafianos, S.; Tuske, S.; Patel, J.; Jansen, R.; Irschik, H.; Arnold, E.; Ebright, R. H. The RNA polymerase "switch region" is a target for inhibitors. *Cell* **2008**, *135* (2), 295−307.

(10) Molodtsov, V.; Fleming, P. R.; Eyermann, C. J.; Ferguson, A. D.; Foulk, M. A.; McKinney, D. C.; Masse, C. E.; Buurman, E. T.; Murakami, K. S. X-ray crystal structures of Escherichia coli RNA polymerase with switch region binding inhibitors enable rational design of squaramides with an improved fraction unbound to human plasma protein. *J. Med. Chem.* **2015**, *58* (7), 3156−71.

(11) Haupenthal, J.; Kautz, Y.; Elgaher, W. A. M.; Patzold, L.; Rohrig, T.; Laschke, M. W.; Tschernig, T.; Hirsch, A. K. H.; Molodtsov, V.; Murakami, K. S.; Hartmann, R. W.; Bischoff, M. Evaluation of Bacterial RNA Polymerase Inhibitors in a Staphylococcus aureus-Based Wound Infection Model in SKH1Mice. *ACS Infect Dis* **2020**, *6* (10), 2573−2581.

(12) Jordheim, L. P.; Durantel, D.; Zoulim, F.; Dumontet, C. Advances in the development of nucleoside and nucleotide analogues for cancer and viral diseases. *Nat. Rev. Drug Discovery* **2013**, *12* (6), 447−464.

(13) Thomson, J. M.; Lamont, I. L. Nucleoside Analogues as Antibacterial Agents. *Front Microbiol* **2019**, *10*, 952.

(14) Maffioli, S. I.; Sosio, M.; Ebright, R. H.; Donadio, S. Discovery, properties, and biosynthesis of pseudouridimycin, an antibacterial nucleoside-analog inhibitor of bacterial RNA polymerase. *J. Ind. Microbiol Biotechnol* **2019**, *46* (3−4), 335−343.

(15) Maffioli, S. I.; Zhang, Y.; Degen, D.; Carzaniga, T.; Del Gatto, G.; Serina, S.; Monciardini, P.; Mazzetti, C.; Guglierame, P.; Candiani, G.; Chiriac, A. I.; Facchetti, G.; Kaltofen, P.; Sahl, H. G.; Deho, G.; Donadio, S.; Ebright, R. H. Antibacterial Nucleoside-Analog Inhibitor of Bacterial RNA Polymerase. *Cell* **2017**, *169* (7), 1240−1248.

(16) Chellat, M. F.; Riedl, R. Pseudouridimycin: The First Nucleoside Analogue That Selectively Inhibits Bacterial RNA Polymerase. *Angew. Chem., Int. Ed. Engl.* **2017**, *56* (43), 13184−13186.

(17) Kunthavai, P. C.; Kannan, M.; Ragunathan, P. Structural analysis of alternate sigma factor ComX with RpoC, RpoB and its cognate CIN promoter reveals a distinctive promoter melting mechanism. *J. Biomol Struct Dyn* **2022**, *40* (14), 6272−6285.

(18) Jorgensen, W. L.; Tirado-Rives, J. The OPLS [optimized potentials for liquid simulations] potential functions for proteins, energy minimizations for crystals of cyclic peptides and crambin. *J. Am. Chem. Soc.* **1988**, *110* (6), 1657−1666.

(19) Madhavi Sastry, G.; Adzhigirey, M.; Day, T.; Annabhimoju, R.; Sherman, W. Protein and ligand preparation: parameters, protocols, and influence on virtual screening enrichments. *J. Comput. Aided Mol. Des.* **2013**, *27* (3), 221−34.

(20) Sherman, W.; Beard, H. S.; Farid, R. Use of an induced fit receptor structure in virtual screening. *Chem. Biol. Drug Des* **2006**, *67* (1), 83−4.

(21) Van Der Spoel, D.; Lindahl, E.; Hess, B.; Groenhof, G.; Mark, A. E.; Berendsen, H. J. GROMACS: fast, flexible, and free. *Journal of computational chemistry* **2005**, *26* (16), 1701−18.

(22) Schuttelkopf, A. W.; van Aalten, D. M. PRODRG: a tool for high-throughput crystallography of protein-ligand complexes. *Acta Crystallogr. D Biol. Crystallogr.* **2004**, *60* (8), 1355−63.

(23) Lindahl, E.; Hess, B.; van der Spoel, D. GROMACS 3.0: a package for molecular simulation and trajectory analysis. *Molecular modeling annual* **2001**, *7* (8), 306−317.

(24) Hess, B.; Kutzner, C.; van der Spoel, D.; Lindahl, E. GROMACS 4: Algorithms for Highly Efficient, Load-Balanced, and Scalable Molecular Simulation. *J. Chem. Theory Comput* **2008**, *4* (3), 435−47.

(25) Parrinello, M.; Rahman, A. J. J. o. A. p. *Polymorphic transitions in single crystals: A new molecular dynamics method.* **1981**, *52* (12), 7182−7190.

(26) Amadei, A.; Linssen, A. B.; Berendsen, H. J. Essential dynamics of proteins. *Proteins* **1993**, *17* (4), 412−25.

(27) Maisuradze, G. G.; Leitner, D. M. Free energy landscape of a biomolecule in dihedral principal component space: Sampling convergence and correspondence between structures and minima. *Proteins: Struct., Funct., Bioinf.* **2007**, *67* (3), 569−578.

(28) Kumari, R.; Kumar, R.; Open Source Drug Discovery, C.; Lynn, A. g_mmpbsa-a GROMACS tool for high-throughput MM-PBSA calculations. *J. Chem. Inf. Model.* **2014**, *54* (7), 1951−62.

(29) Gasteiger, E.; Hoogland, C.; Gattiker, A.; Duvaud, S. e.; Wilkins, M. R.; Appel, R. D.; Bairoch, A. Protein Identification and Analysis Tools on the ExPASy Server. In *The Proteomics Protocols Handbook*; Walker, J. M., Ed.; Humana Press: Totowa, NJ, 2005; pp 571−607.
(30) Perez-Iratxeta, C.; Andrade-Navarro, M. A. J. B. s. b. K2D2: estimation of protein secondary structure from circular dichroism spectra. *BMC Struct. Biol.* **2008**, *8* (1), 25.
(31) Geourjon, C.; Deleage, G. SOPMA: significant improvements in protein secondary structure prediction by consensus prediction from multiple alignments. *Comput. Appl. Biosci* **1995**, *11* (6), 681−4.
(32) Lakshmi, T. P.; Moumita, M.; Krishna, R.; Sakthivel, N. Molecular interaction of 2,4-diacetylphloroglucinol (DAPG) with human serum albumin (HSA): The spectroscopic, calorimetric and computational investigation. *Spectrochim. Acta A Mol. Biomol. Spectrosc.* **2017**, *183*, 90−102.
(33) Brown, R. K.; Brandts, J. M.; O'Brien, R.; Peters, W. B. ITC-derived binding constants: Using microgram quantities of protein. In *Label-Free Biosensors: Techniques and Applications*; Cooper, M. A., Ed.; Cambridge University Press: Cambridge, 2009; pp 223−250.
(34) Dunitz, J. D. Win some, lose some: enthalpy-entropy compensation in weak intermolecular interactions. *Chem. Biol.* **1995**, *2* (11), 709−12.
(35) Du, X.; Li, Y.; Xia, Y. L.; Ai, S. M.; Liang, J.; Sang, P.; Ji, X. L.; Liu, S. Q. Insights into Protein-Ligand Interactions: Mechanisms, Models, and Methods. *Int. J. Mol. Sci.* **2016**, *17* (2), 144.
(36) Celej, M. S.; Dassie, S. A.; Freire, E.; Bianconi, M. L.; Fidelio, G. D. Ligand-induced thermostability in proteins: thermodynamic analysis of ANS-albumin interaction. *Biochim. Biophys. Acta* **2005**, *1750* (2), 122−33.
(37) Pawar, S. K.; Jaldappagari, S. Interaction of repaglinide with bovine serum albumin: Spectroscopic and molecular docking approaches. *J. Pharm. Anal* **2019**, *9* (4), 274−283.
(38) Kelly, S. M.; Price, N. C. The use of circular dichroism in the investigation of protein structure and function. *Curr. Protein Pept Sci.* **2000**, *1* (4), 349−84.
(39) Adler, A. J.; Greenfield, N. J.; Fasman, G. D. Circular dichroism and optical rotatory dispersion of proteins and polypeptides. *Methods Enzymol* **1973**, *27*, 675−735.
(40) Xu, H.; Gao, S.-L.; Lv, J.-B.; Liu, Q.-W.; Zuo, Y.; Wang, X. Spectroscopic investigations on the mechanism of interaction of crystal violet with bovine serum albumin. *J. Mol. Struct.* **2009**, *919* (1), 334−338.
(41) Ding, L.; Zhou, P.; Zhan, H.; Zhao, X.; Chen, C.; He, Z. Systematic investigation of the toxicity interaction of ZnSe@ZnS QDs on BSA by spectroscopic and microcalorimetry techniques. *Chemosphere* **2013**, *92* (8), 892−7.
(42) Shi, J.-H.; Chen, J.; Wang, J.; Zhu, Y.-Y.; Wang, Q. Binding interaction of sorafenib with bovine serum albumin: Spectroscopic methodologies and molecular docking. *Spectrochimica Acta Part A: Molecular and Biomolecular Spectroscopy* **2015**, *149*, 630−637.
(43) Hui, Y.; Xue, X.; Xuesong, Z.; Yan, W. Intrinsic Fluorescence Spectra of Tryptophan, Tyrosine and Phenyloalanine. In *Proceedings of the 5th International Conference on Advanced Design and Manufacturing Engineering*; Atlantis Press, 2015; pp 224−233.
(44) Lakowicz, J. *Lakowicz JR (2006) Principles of fluorescence spectroscopy*, 3rd ed.; Springer: New York, 2006.

https://doi.org/10.1021/acsomega.2c07805
ACS Omega 2023, 8, 7989−8000